# CBELSA/TAPS Analysis Note:
# $\gamma p \rightarrow p\omega$

Andrew Wilson
Florida State University
Tallahassee, Florida USA
awilson@hadron.physics.fsu.edu

November 18, 2011

This paper is a concise description of the analysis of the reaction $\gamma p \rightarrow p\omega$ using events from the CBELSA/TAPS experiment in its October to November 2002 configuration. An unpolarized photon beam from 0.7 to 3.2 GeV was incident on a target of unpolarized liquid hydrogen.

## Contents

# List of Figures

# 1 Differential Cross Sections

The results from this analysis are presented in Figures 1, 2, and 3. Figure 1 presents the data in the familiar angular differential cross section. Figure 2 emphasizes the energy evolution of the differential cross sections. As can be seen seen from the cross sections, the differential cross section is forward peaked and suggests that a t-channel process becomes dominant at higher energies. To show this, the SAPHIR experiment previously measured the differential cross sections as a function of the Mandelstam t variable. To compare, the same distributions were produced from these data and are presented in Figure 3.

The forward region ($\cos\theta^{\omega}_{c.m.} > 0.8$) has been broken down into a finer binning to show the rapid increase in the differential cross section in this region. The CLAS data in the $\cos\theta^{\omega}_{c.m.} = 0.833-0.866$ bin in Figure 2 was actually measured over the range $\cos\theta^{\omega}_{c.m.} = 0.8 - 0.9$, but strictly these data points can interpreted as the average differential cross section at $\cos\theta^{\omega}_{c.m.} = 0.85$. To try to compare in the most fair way, this data point was compared to the corresponding bin.

This analysis features approximately 120,000 $\omega$'s in the reconstruction of the data events. The possible background reaction contributions seem to be negligible (Section 5) and the differential cross section features a strong forward angle rise at higher energies (Section 4). This data should add new information about the forward angles and help to fix the t-channel contributions. These t-channel contributions should be fixed to properly extract the underlying resonance contribution.

The rest of this paper will be devoted to describing the analysis that lead to these results. In Section 2, The kinematic cuts and background subtraction are described. In Section 3, the differential cross sections are compared to earlier measurements. The possible background reactions that could be diluting the signal in this analysis is studied in Section 5. The possible sources of systematic errors are presented in Section 6. Finally, Section 7 shows plots that do not lead to modifications to the analysis, but are important to understanding the data.

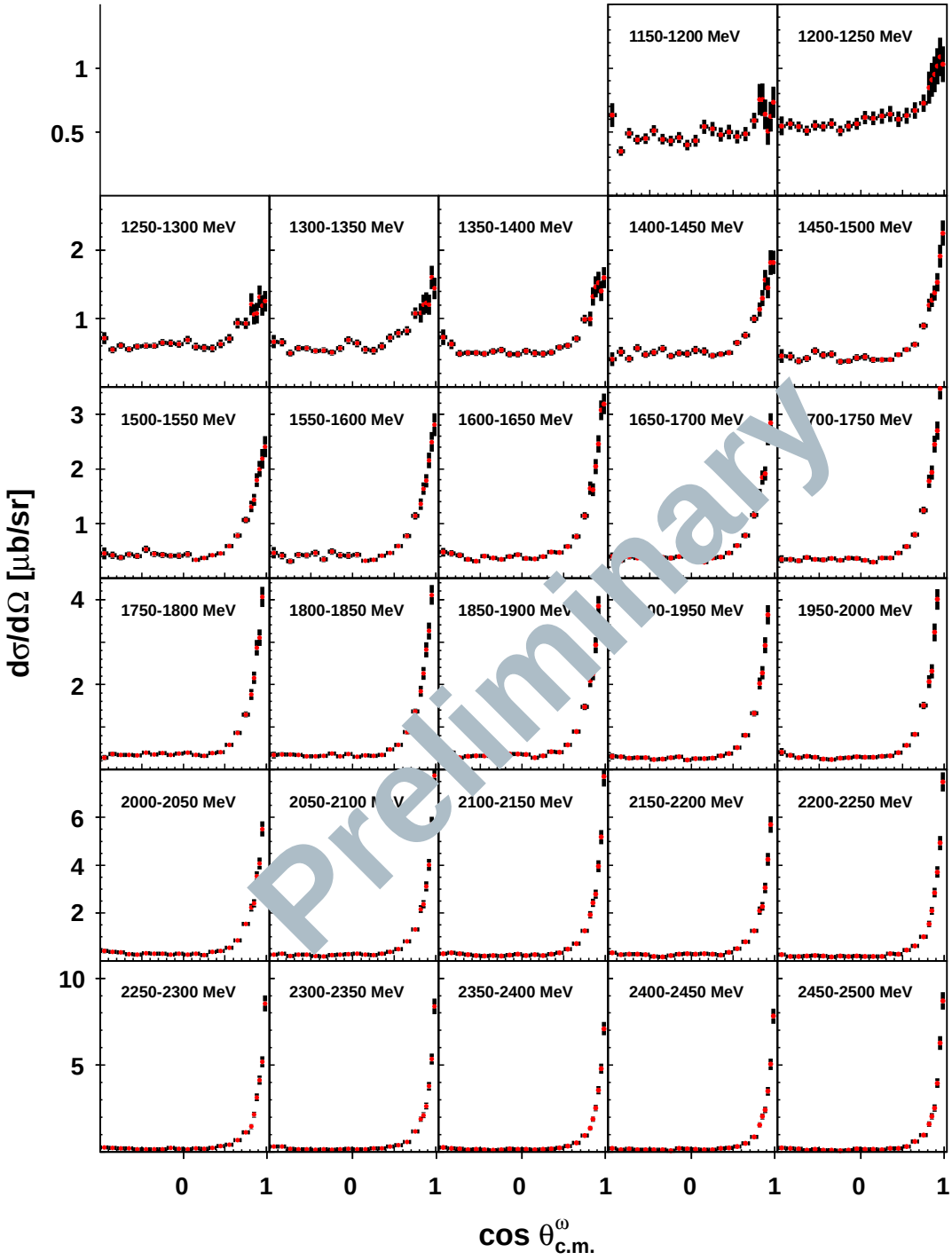


Figure 1: Angular Differential Cross Section. Each histogram is labeled with its range in incoming photon energy and the horizontal axis is binned in the center of mass angle of the $\omega$ meson. Statistical errors only.

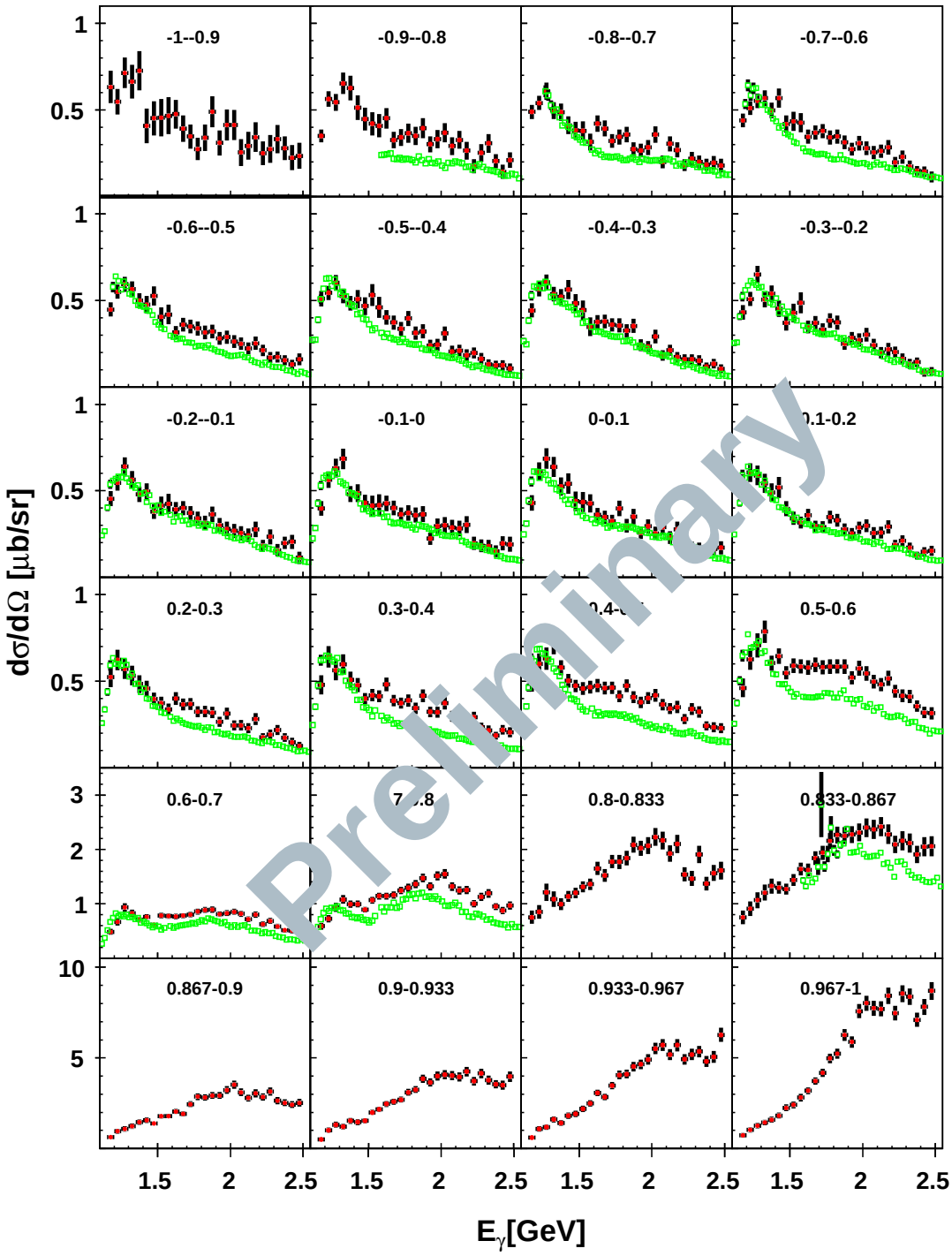


Figure 2: $\gamma p \to p\omega$ Excitation Function. Each histogram in labeled with its range in $\cos\theta^{\omega}_{c.m.}$ and the horizontal axis is binned in incoming photon energy. The green points are from CLAS and the red points are from this analysis. Statistical errors only.

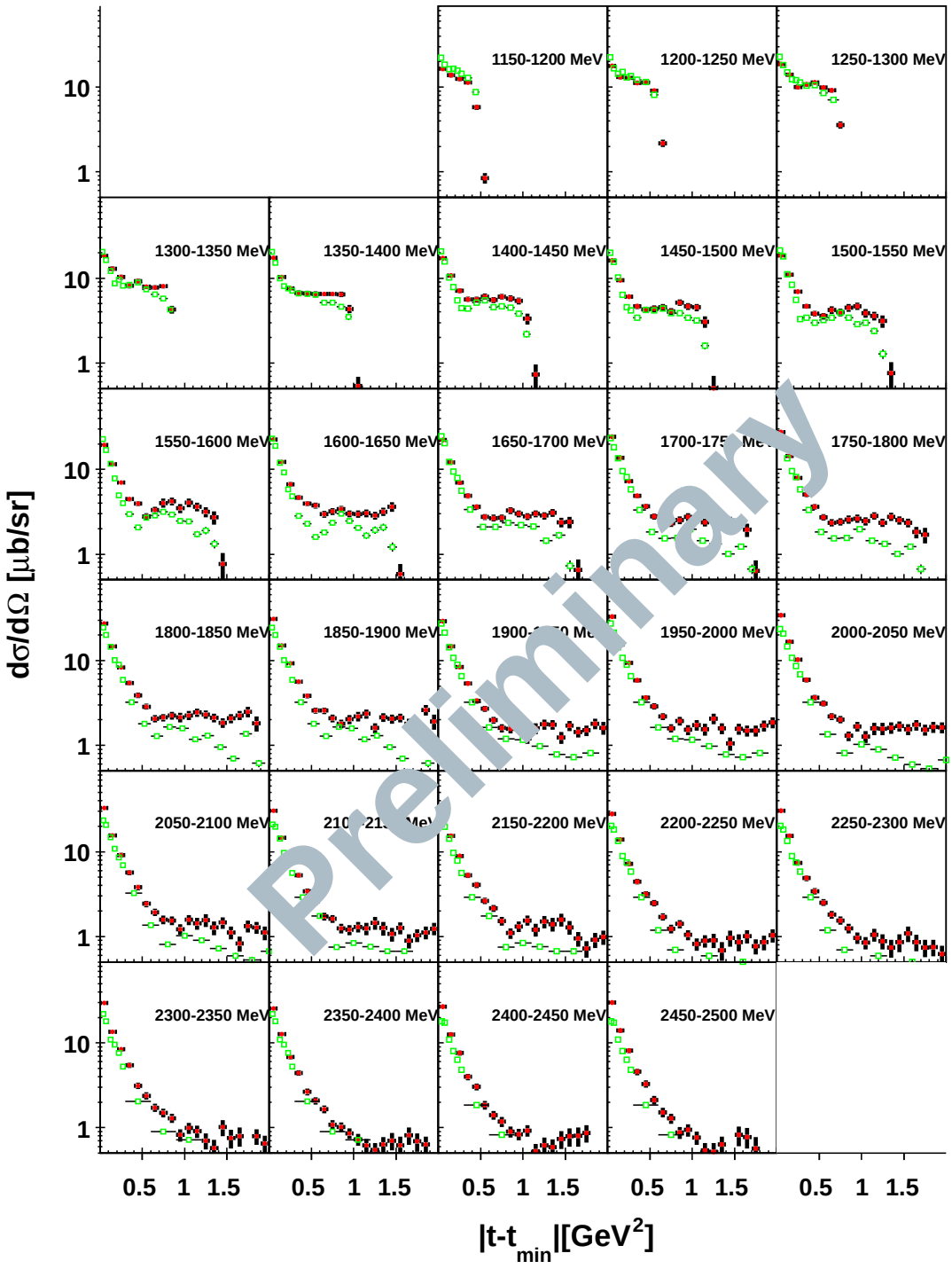


Figure 3: Mandelstam t Differential Cross Sections. Each histogram is labeled with its range in incoming photon energy and is binned in the Mandelstam t variable. The green points are from SAPHIR and the red points are from this analysis. Statistical errors only.

# 2 Kinematic Cuts and Background Subtraction

In this section, the reconstruction and isolation of the desired $\gamma p \to p\omega$ events are described.

## 2.1 Initial Cuts

The only CBELSA/TAPS detectable final state with a significant branching ratio (8.9%) that decays from the $p\omega$ final state is

$$p\omega \to p(\pi^0\gamma) \to p(\gamma\gamma)\gamma \to 3/4PEDs$$

.

Initial Kinematic Cuts

| Cut Type | Inclusive Cut Value |
|---|---|
| Uncharged PEDs | 3 |
| Charged PEDs | 0 or 1 |
| Coplanarity | $\pm 30deg$ |
| Uncharged time | $\pm 3ns$ |
| Charged time | $\{-5, +15ns\}$ |
| Confidence Level($p_{miss}\pi^0\gamma$)(Fig. 6) | >0.005 |

The resulting $\pi^0\gamma$ invariant mass histogram, from data events, is shown in Figure 4. The resulting $\gamma\gamma$ invariant mass histogram, from the surviving data events and using the unfitted vectors, is shown in Figure 5. The confidence level distribution for fitting to the $p_{missing}\pi^0\gamma$ final state is shown in Figure 6.

Figure 5 shows some unwanted contribution from $\eta$ mesons. This seems to be from the $p\pi^0\eta$ final state. Monte Carlo simulated $p\pi^0\eta$ events were subjected to the same initial kinematic cuts and Figure 7 shows the resulting $\gamma\gamma$ invariant mass, where the same eta peak is visible.

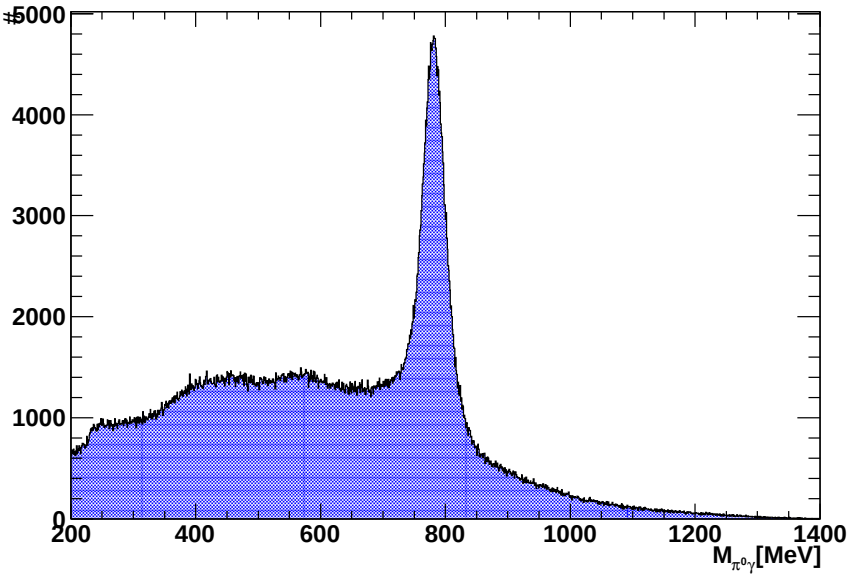


Figure 4: $\pi^0\gamma$ Invariant Mass after initial kinematic cuts. The structures to the left of the $\omega$ peak seem to be from hadronic background where one or more photons have been lost.

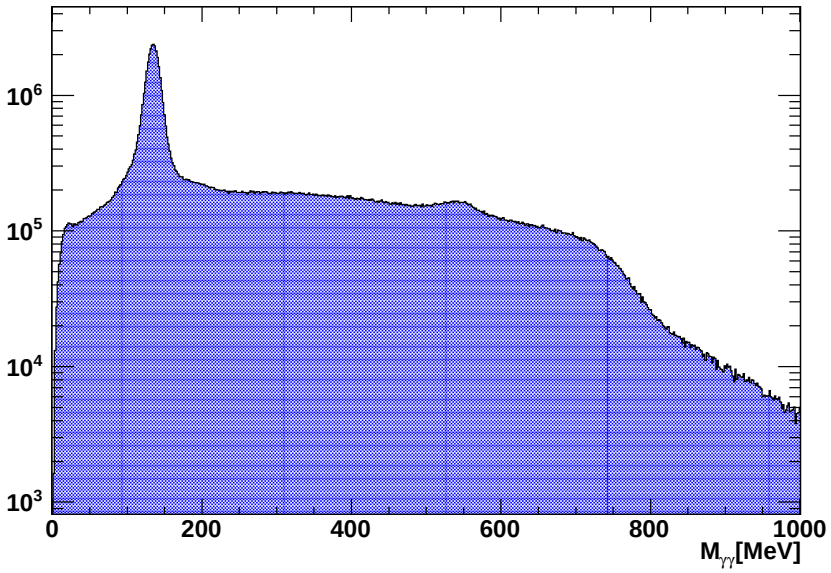


Figure 5: $\gamma\gamma$ Invariant Mass, from unfitted vectors, after the kinematic confidence level cut ($CL_{p_{miss}\pi^0\gamma} < 0.005$). Other than the $\pi^0$ peak, there is an unwanted peak corresponding to the $\eta$ meson. There are three contributions to this histogram from each event.

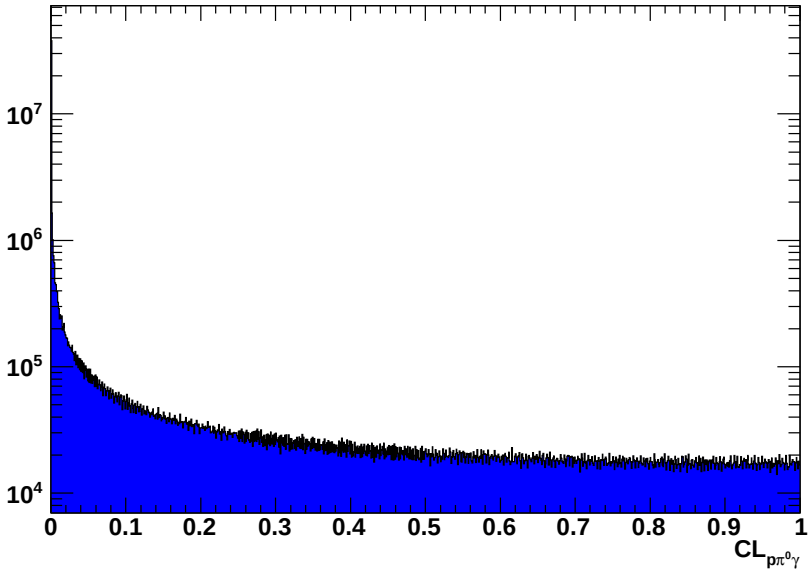


Figure 6: Confidence Level distribution for the kinematic fit to $p_{miss}\pi^0\gamma$.

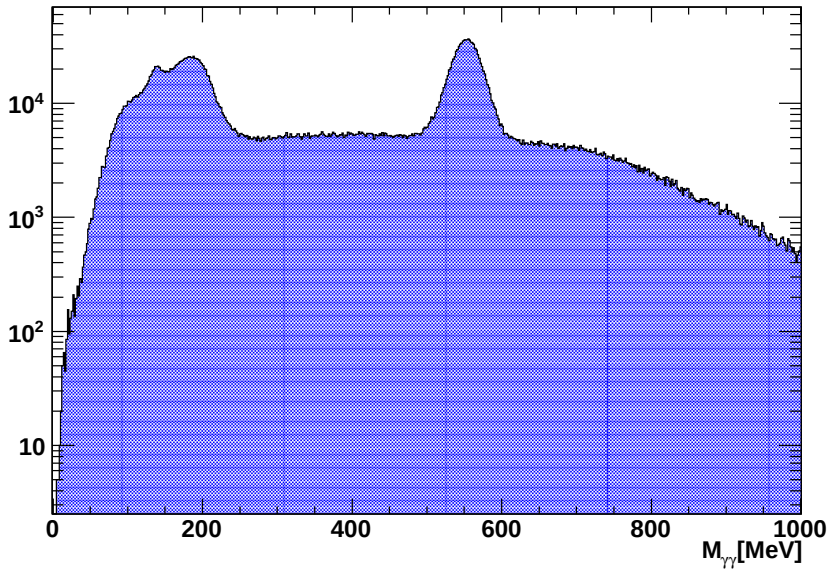


Figure 7: $\gamma\gamma$ Invariant Mass, from unfitted vectors, after the kinematic confidence level cut ($CL_{p_{miss}\pi^0\gamma} < 0.005$) for Monte Carlo Simulated $p\pi^0\eta$ events. There are three contributions to this histogram from each event. Most of the contribution seems to come from a missing $\pi^0$ photon.

## 2.2 Opening Angle Cut

Figure 8 shows the opening angle between the $\pi^0$ meson and the photon in the center of mass frame versus the momentum of the $\omega$ meson. In Figure 8a, there are some features in the distribution at high $\omega$ momentum and large opening angle. For a feeling for where some of the structures come from, Monte Carlo phase space distributed output for possible background reactions were subjected to the same kinematic cuts and reconstructed as $p\omega$ events. From these simulated events, the corresponding opening angle histograms are shown in Figure 9. At least one of the features in Figure 8a are attributed to $p\pi^0$ events(Figure 9a). To reduce the effect of these types of events, a momentum dependent cut on the opening angle was used and is shown in the right column of Figures 8 and 9.

The formula for the cut is all events satisfying

$$|p_\omega^{cms}| > -13.33 * \theta_{\pi^0,\gamma}^{cms} + 2400$$

are cut from the analysis, where $p_\omega^{cms}$ is the momentum of the $\omega$ meson in the center of mass system and $\theta_{\pi^0,\gamma}^{cms}$ is the angle between the $\pi^0$ and the photon in the center of mass system.

This cut was done before background fitting (Qvalue method).

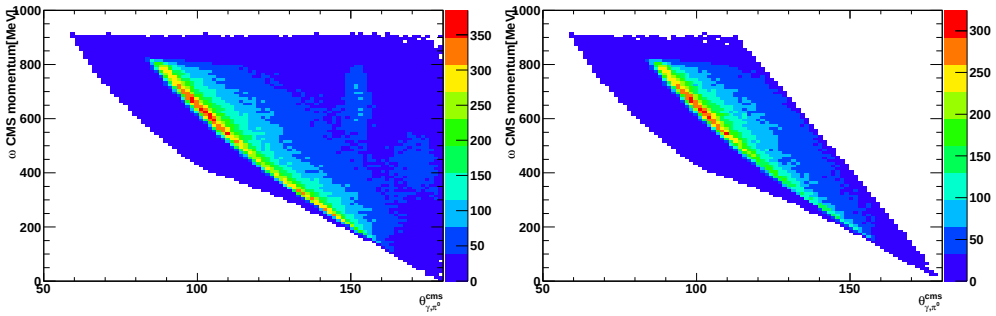


(a) Data before cuts

(b) Data after cuts

(c) $MC_{rec}$ before cuts

(d) $MC_{rec}$ after cuts

Figure 8: Opening Angle Histograms for $p\omega$ data. Opening angle of the reconstructed $\pi^0, \gamma$ system versus momentum of the reconstructed $\omega$ meson in the center of mass system.

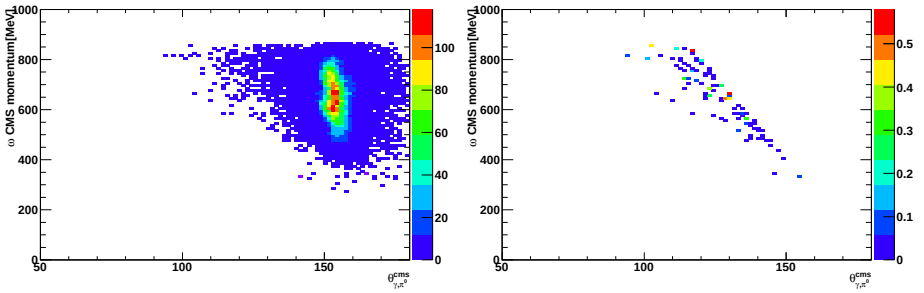


(a) $p\pi^0$ before cuts (b) $p\pi^0$ after cuts

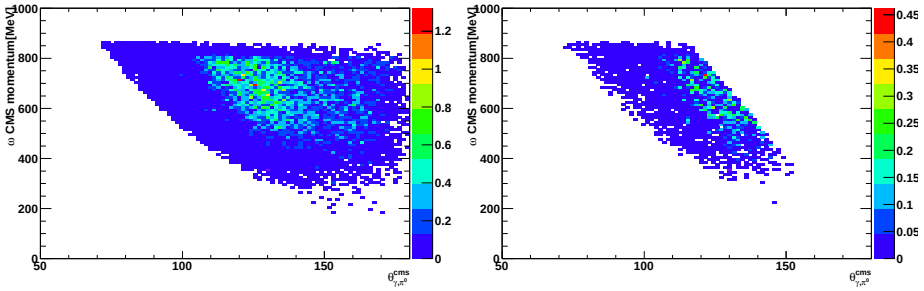


(c) $p\eta$ before cuts (d) $p\eta$ after cuts

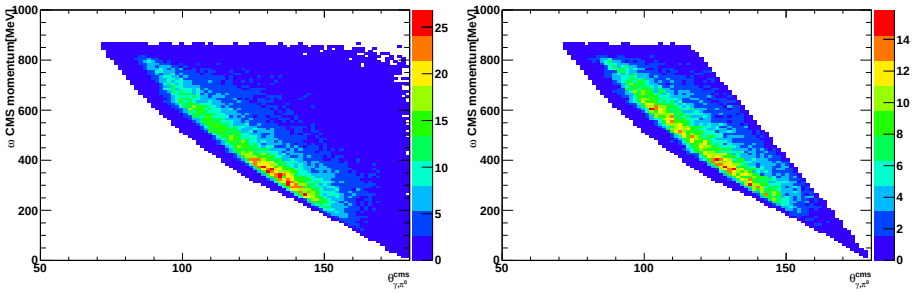


(e) $p\pi^0\pi^0$ before cuts (f) $p\pi^0\pi^0$ after cuts

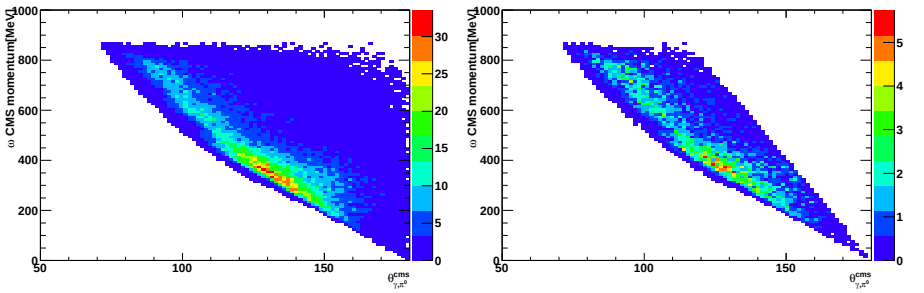


(g) $p\pi^0\eta$ before cuts (h) $p\pi^0\eta$ after cuts

Figure 9: Opening Angle Histograms for Monte Carlo simulated background reactions. Opening angle of the reconstructed $\pi^0, \gamma$ system versus momentum of the reconstructed $\omega$ meson in the center of mass system after being subjected to the same cuts as the $p\omega$ events.

## 2.3 Background Subtraction: QValue Fitting

Since the natural width of the $\omega$ meson (8.49 MeV) is comparable to the resolution of the experiment in measuring invariant masses ($\sim 10MeV$), the $p\omega$ final state could not be reliably kinematically fitted to. Therefore, the $\pi^0\gamma$ invariant mass spectrum must be used to subtract away all the non-$p\omega$ events.

After the initial kinematic cuts, the remaining events were subjected to event-based background subtraction (Qvalue Method) in the $\pi^0\gamma$ invariant mass distribution.

QValue Method

1. Find the 300 nearest neighbor events in the kinematic phase space to each event, which is defined by:
   - Center of Mass energy ($\sqrt{s}$)
   - Cosine of the polar angle of the $\omega$ meson in the center of mass frame. ($\cos\theta^{\omega}_{c.m.}$)
   - Azimuthal angle of the $\omega$ meson in the center of mass frame. ($\phi^{cms}_{\omega}$)
2. Plot these events in the $\pi^0\gamma$ invariant mass distribution.
3. Fit this distribution with $f(x) = D[f_s S + (1 - f_s)(C * A)]$
   - Overall constant D fitted.
   - Signal fraction $f_s$ fitted between 0 - 1.
   - signal function (Voigt function) $S$
     - Width fixed to 8.49 MeV. (PDG Value)
     - Sigma fitted between 7 - 50 MeV
     - Mean fitted between 757 - 807 MeV
   - 1st order Chebychev polynomial $C$
     - 0th order constant fixed to 1.
     - 1st order constant fitted between -10 - 10 .
   - Argus Background Function $A$ (Figure 10)
     - cut off parameter ($m0$) fitted within 20 MeV of the largest $\pi^0\gamma$ mass value.
     - curvature parameter ($c$) fixed to $-1 \times 10^{-7}$ .
4. Used fit to define Qvalue (the probability that this event is a signal event.)
5. Repeat for each event with a $\pi^0\gamma$ invariant mass between 600 and 1100 MeV.

The mass fitting was done using the Roofit package and done in an unbinned maximum likelihood fit. The Voigt function was used to fit the signal due to the fact that the width of the $\omega$ meson has a natural width that is on the same order of resolution as the detector system. The Voigt function is a convolution of a Breit-Wigner function and a Gaussian function.

The Argus Background Function is used because, in many of these distributions, the end of phase space is encountered in proximity to the $\omega$ peak. The Argus function was developed to

model the edge of phase space in a mass distribution by the ARGUS experiment. An example of the Argus function is shown in Figure 10. The functional form of the Argus function is

$$f(x, m0, c) = x(1 - (\frac{x}{m0})^2)^{0.5} * \exp(c(1 - (\frac{x}{m0})^2)))$$

. This function was also previously used at CLEO and BaBar experiments.

Qvalue fit examples can be found in Figure 11. After the fit, the Qvalue is defined as

$$Q_{event} = \frac{f_s S(x_{event})}{f_s S(x_{event} + (1 - f_s)(A(x_{event}) * C(x_{event}))}$$

where $x_{event} = M^{event}_{\pi^0\gamma}$. The $M^{event}_{\pi^0\gamma}$ is the value of the original event's value in the $M_{\pi^0\gamma}$ distribution. Here the original event means the event that is going to be assigned the Qvalue to.

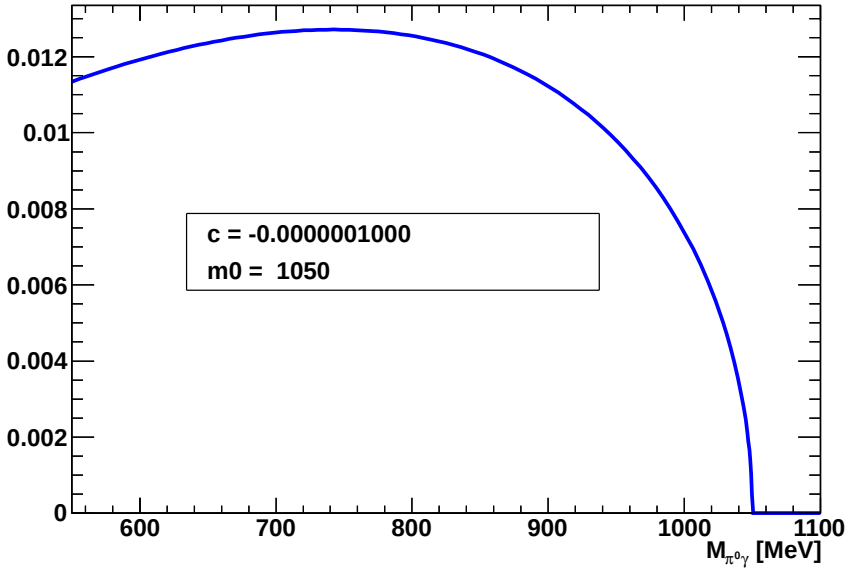


Figure 10: Example of an Argus Function. The c parameter is the same as in each of the fits in this analysis. The m0 parameter is fitted to the data.

After Qvalue fitting, all events are stored with their Qvalue, which will be used to weight each event upon plotting. This also allows the opportunity to explore any additional event by event cuts while immediately seeing the effect on the differential cross sections and other distributions without refitting. In this way, its much easier to investigate the effects of additional cuts due to the fact that plotting only takes the time to add up the contributions from each event.

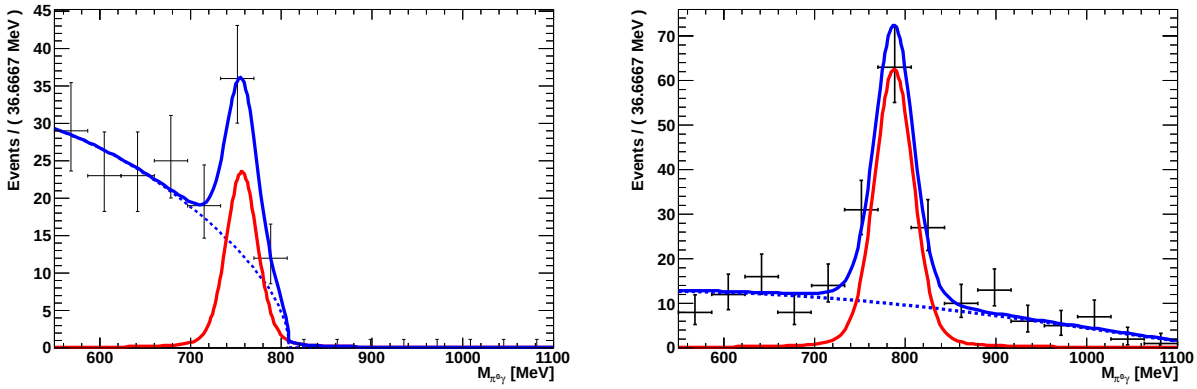


(a) Low Energy Fit

(b) High Energy Fit

Figure 11: Example of Qvalue Fits. Left figure is from a fit of low energy data ($1100MeV < E_\gamma < 1150MeV$). Right figure is from a fit of high energy data ($2450MeV < E_\gamma < 2500MeV$). The blue solid curve is the total function. The red solid curve is the signal function (Voigt). The blue dashed curve is the background function (Argus*Chebychev).

## 2.4 Qvalue Error Determination and Propagation

In order to properly represent these Qvalues, the systematic errors must be estimated due to the fact that each Qvalue is actually a function of all the events used in the fit to determine the value. The errors defined in the fit must be propagated to the Qvalue itself. This is done by estimating the error of each parameter that is fixed by the fit and propagating it to the Qvalue. The formula to estimate a Qvalue's error is

$$\sigma_Q^2 = \sum_{ij} \frac{\partial Q}{\partial \alpha_i} (C_\alpha)_{ij} \frac{\partial Q}{\partial \alpha_j}$$

, where $\alpha$ is one of the fitted parameters and $(C_\alpha)_{ij}$ is the covariance matrix. The covariance matrix is obtained directly from the Roofit fitter. The derivatives are easily either analytically calculated or numerically determined.

Propagation to the final plots (as in Figure 2), the following propagation formula

$$\sigma_y^2 = \sum_{ij} \sigma_Q^i \rho_{ij} \sigma_Q^j$$

is used, where $\rho_{ij}$ is the correlation matrix. A correlation factor between two Qvalues is equal the fraction of nearest neighbor events (Qvalue Method table item 1).

## 2.5 Trigger Cut

The final cut which is done after Qvalue fitting is the trigger cut defined by throwing out any event where there is exactly one photon and a reconstructed proton in the TAPS detector, while the trigger for two low energy hits in TAPS fired and no other trigger did. This cut is only done close to the $p\omega$ threshold ($E_\gamma < 1.5GeV$).

Trigger Conditions

- 2 Low Energy Hits in TAPS
- 1 High Energy Hit in FACE and 1 High Energy Hit in TAPS

When triggering on the proton, the TAPS detector does not always reliably record a particle energy deposit above the threshold for triggering. When there is one proton and one photon that are in different segments of the low energy trigger, there seems to be effects in the measured cross section that are unphysical. At higher energies more than 400 MeV above threshold, the proton has enough kinetic energy and records a particle energy deposit. This effect can be seen when comparing between Figures 12b and 12c in the low energy region.

### 2.6 Cut Effects

After all cuts, there were approximately 120,000 $\omega$'s found in the analysis. The remaining events, weighted with it's Qvalue, are used to form the differential cross sections presented in Figures 1, 2, and 3.

The final $\pi^0\gamma$ invariant mass distribution is shown in Figure 13, where the background is shown. Figure 14 shows the effect of each cut on the $\pi^0\gamma$ invariant mass spectrum.

The relative effect on the differential cross section from each of the last few cuts are shown in Figure 12.

Figure 15 is presented to contrast against Figure 5 after all cuts are done. The most notable development is the disappearance of the $\eta$ peak. This indicates that the contribution from $p\pi^0\eta$ has been rendered negligible. This is discussed further in Section 5. The factor that most likely reduces the $p\pi^0\eta$ contribution is the combination of the opening angle cut and background subtraction.

For an overall look at how the two photon invariant mass relates to the overall three photon invariant mass, Figure 16 is presented for both the events present before the $p_{miss}\pi^0\gamma$ confidence level $> 0.005$ cut and for the events after all cuts and background subtraction.

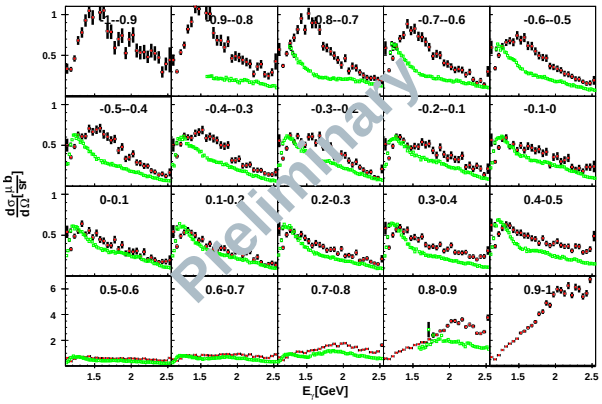


(a) No Cuts

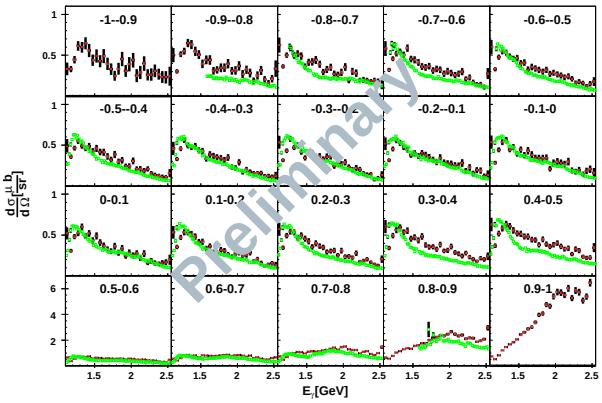


(b) After Opening Angle Cut

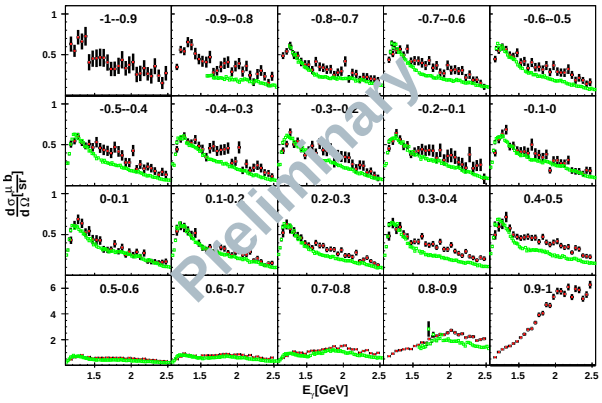


(c) After Trigger Cut ($E_\gamma < 1.5GeV$) (Final)

Figure 12: $\gamma p \to p\omega$ Excitation Functions. (Consolidated View.) Each histogram in labeled with its range in $\cos\theta^{\omega}_{c.m.}$ and the horizontal axis is binned in incoming photon energy. The green points are from CLAS and the red points are from this analysis. Statistical errors only.

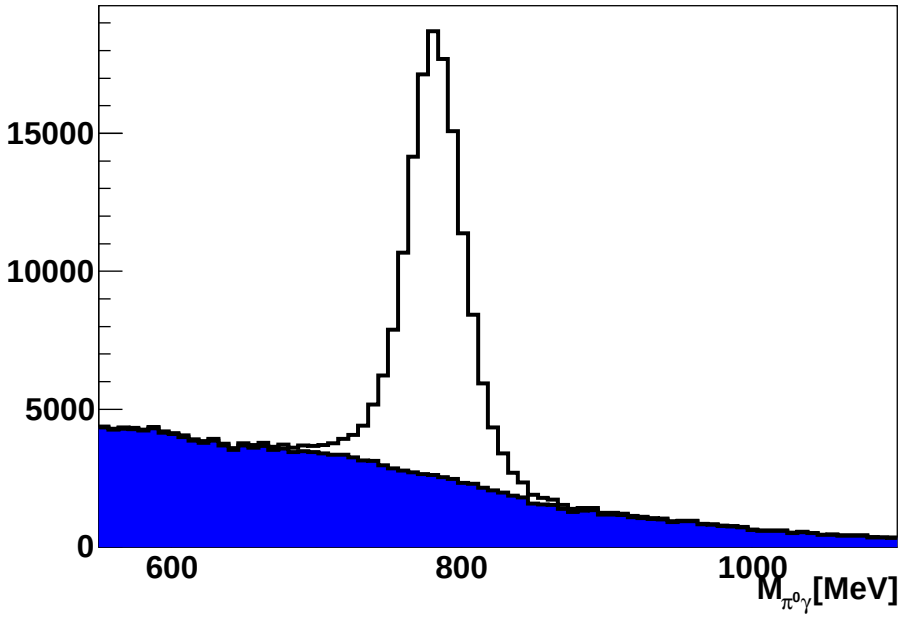


Figure 13: Total $\pi^0\gamma$ Invariant Mass Distribution. The solid blue shows the background that is subtracted using the Qvalue method. There were approximately 120,000 $\omega$'s in this analysis.

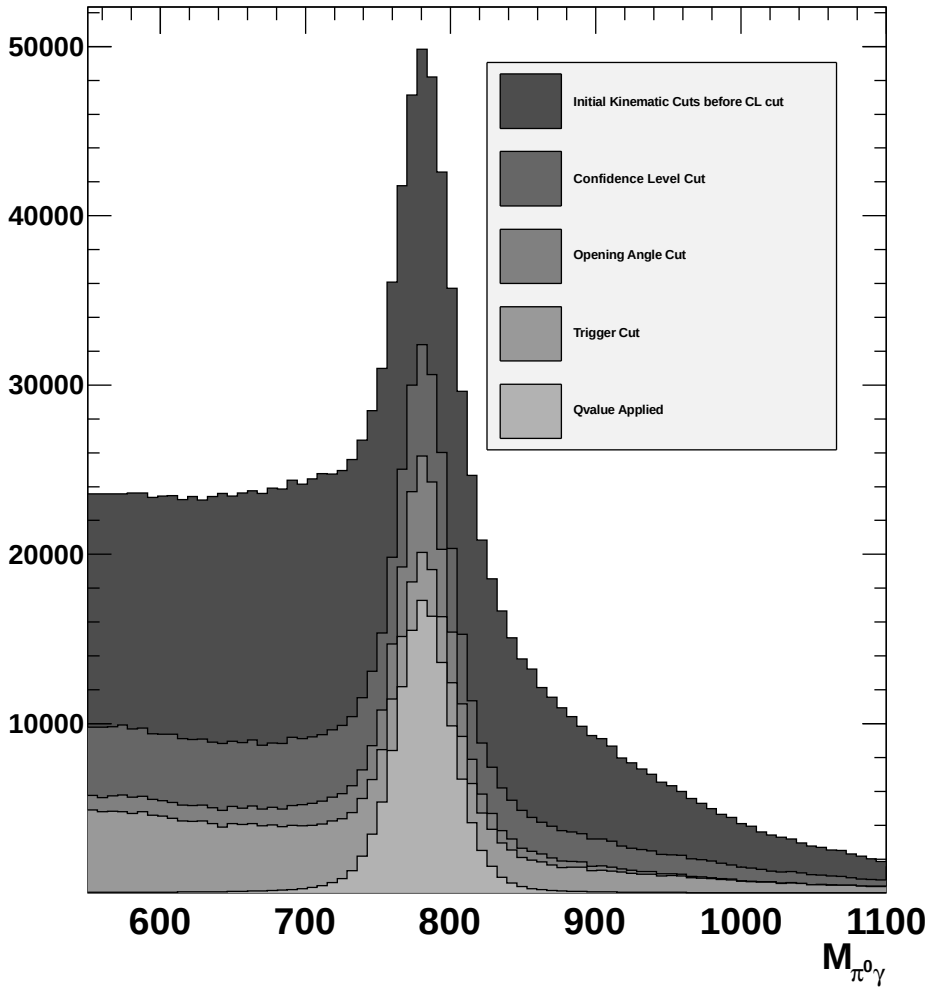


Figure 14: Total $\pi^0\gamma$ Invariant Mass Distribution Evolution. The binning in this histogram is much more coarse than in Figure 4.

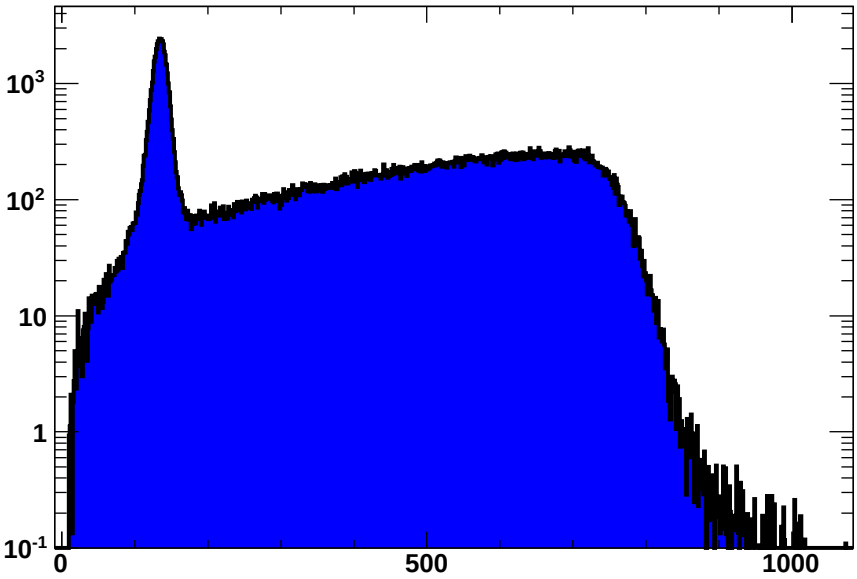


Figure 15: Total $\gamma\gamma$ Invariant Mass Distribution After Cuts. This is for all events used in forming the differential cross section. There are three entries for each event. Notice the $\eta$ peak from Figure 5 is no longer present.

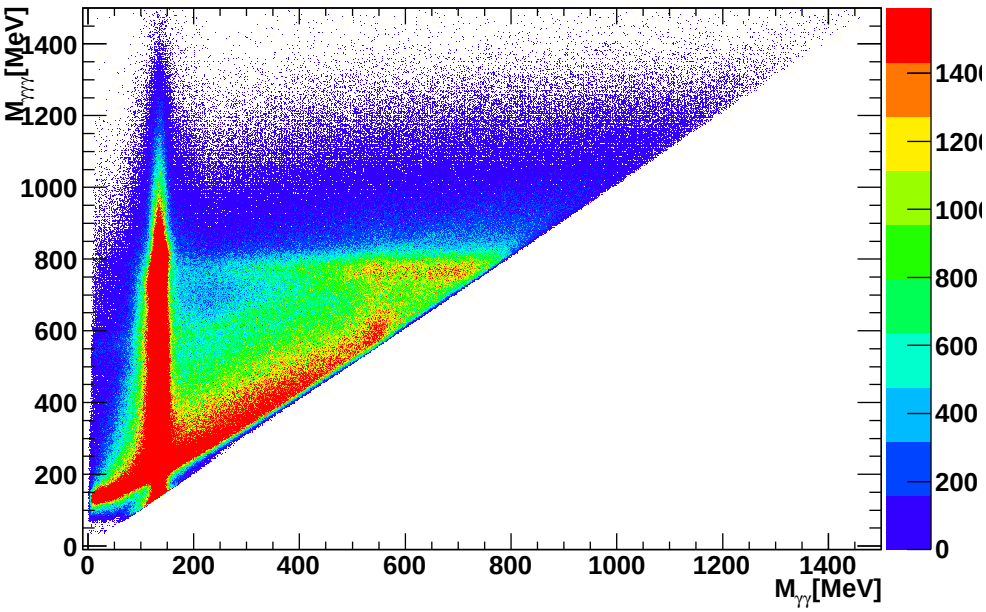


(a) Before Confidence Level Cut

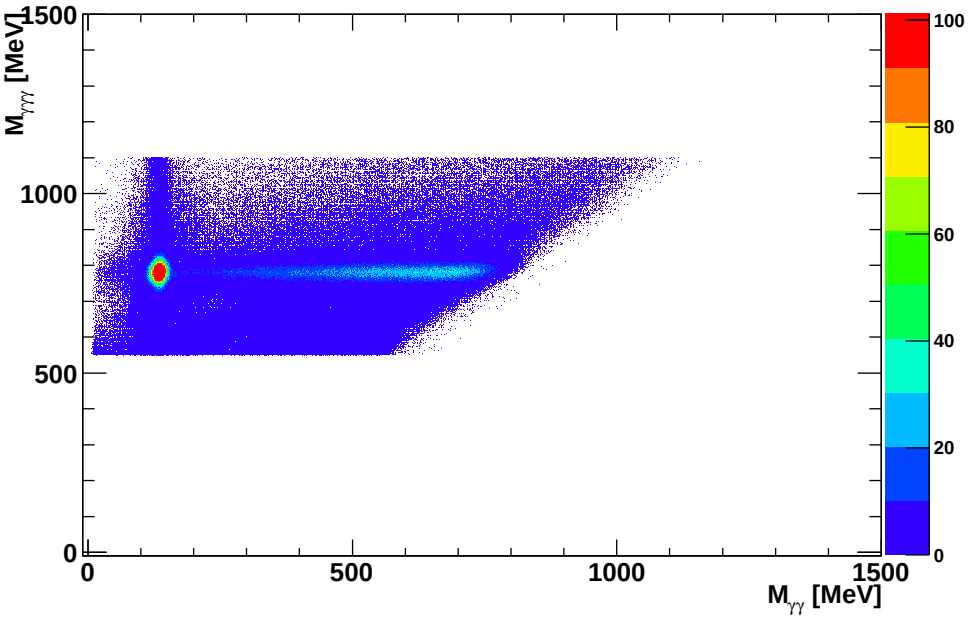


(b) After Background Subtraction and All Cuts

Figure 16: $M_{\gamma\gamma}$ vs $M_{\gamma\gamma\gamma}$ Distribution Evolution. This is for all events used in forming the differential cross section. There are three entries for each event.

# 3 CLAS and SAPHIR comparisons

This data and the corresponding CLAS data are shown in Figure 2 and seem to have similar overall shapes. The ratio between these two data sets are shown in Figure 17. Figure 17 shows that this data is slightly higher at higher energies than the CLAS data on the order of about 20-30% over most of the range. This difference looks like a normalization issue.

This data and the corresponding SAPHIR data are shown in Figure 3. The ratio of the first three CBELSA/TAPS bins in each histogram are shown in Figure 18. These three bins correspond to the forward scattering angles in Figure 2 and show a comparison to the data points that are missing from the CLAS comparison. There seems to be a 40% discrepancy at higher energies.

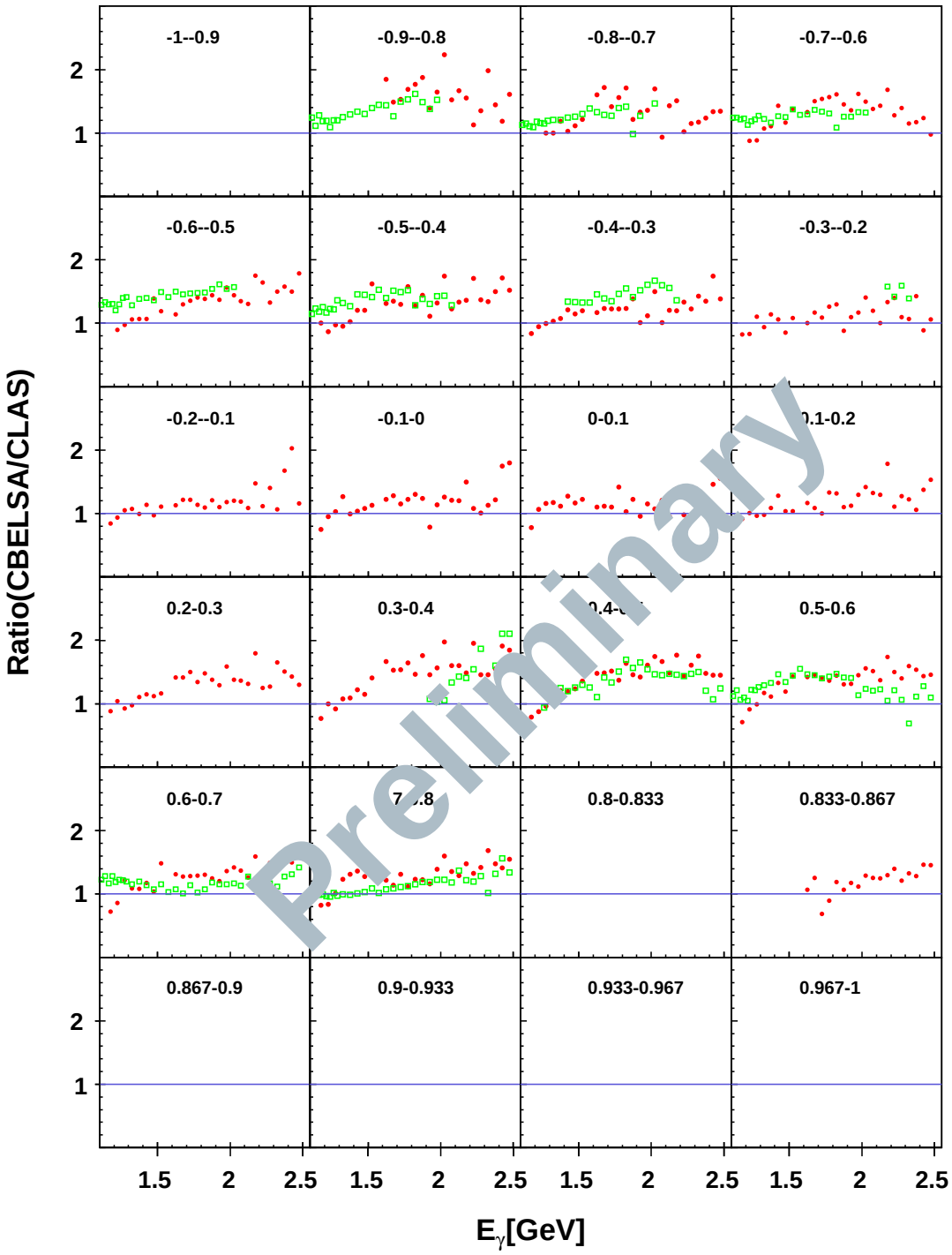


Figure 17: Ratio of CBELSA/TAPS to CLAS Excitation Functions. This ratio uses the data from Figure 2. Each histogram in labeled with its range in $\cos\theta^{\omega}_{c.m.}$ and the horizontal axis is binned in incoming photon energy. The red points are the ratios for this analysis to CLAS. The green points are the corresponding ratios for the $\gamma p \to p\pi^0$ differential cross sections to the CLAS $\gamma p \to p\pi^0$ differential cross sections.

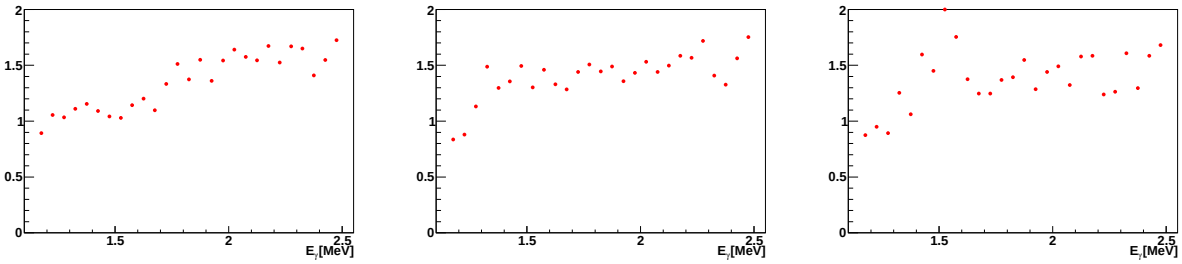


(a) $|t - t_{min}| = 0 - 0.1$ (b) $|t - t_{min}| = 0.1 - 0.2$ (c) $|t - t_{min}| = 0.2 - 0.3$

Figure 18: Ratio of CBELSA/TAPS to SAPHIR from each histogram in Figures 3.

# 4 Forward Angle, High Energy Behavior

In Figure 2, the $\cos\theta_\omega > 0.8$ region has been expanded to show the evolution of the differential cross section in this area. This region seems to rise sharply at forward angles and needs to be checked to build confidence in this result.

Figure 19 shows the Monte Carlo simulated acceptance for this analysis and shows that the acceptance does not change very much over the high energy, forward angle range. Figure 20 shows the fraction of 3 PED events reconstructed in each bin. The reliance on reconstruction changes from 4 PED to 3 PED events in the middle of this range, but it seems that the Monte Carlo models this exchange quite well.

The stability of this region is studied in Figure 21. The confidence level cut in the initial kinematic cuts was varied to study the relative amount of background that contributes to each data point. The hypothesis being that the background contribution to the result should be more sensitive to confidence level than the signal contribution which would cause the result to change. The histograms show that, within the error, the result does not change. This means that either there is negligible background or that the background contribution is invariant to confidence level.

To give a flavor of the dynamics of this region, Figure 22 shows where the decay products are reconstructed. Most of the time the $\pi^0$ meson is reconstructed in TAPS and resembles the reconstruction of $p\pi^0$ events in this region.

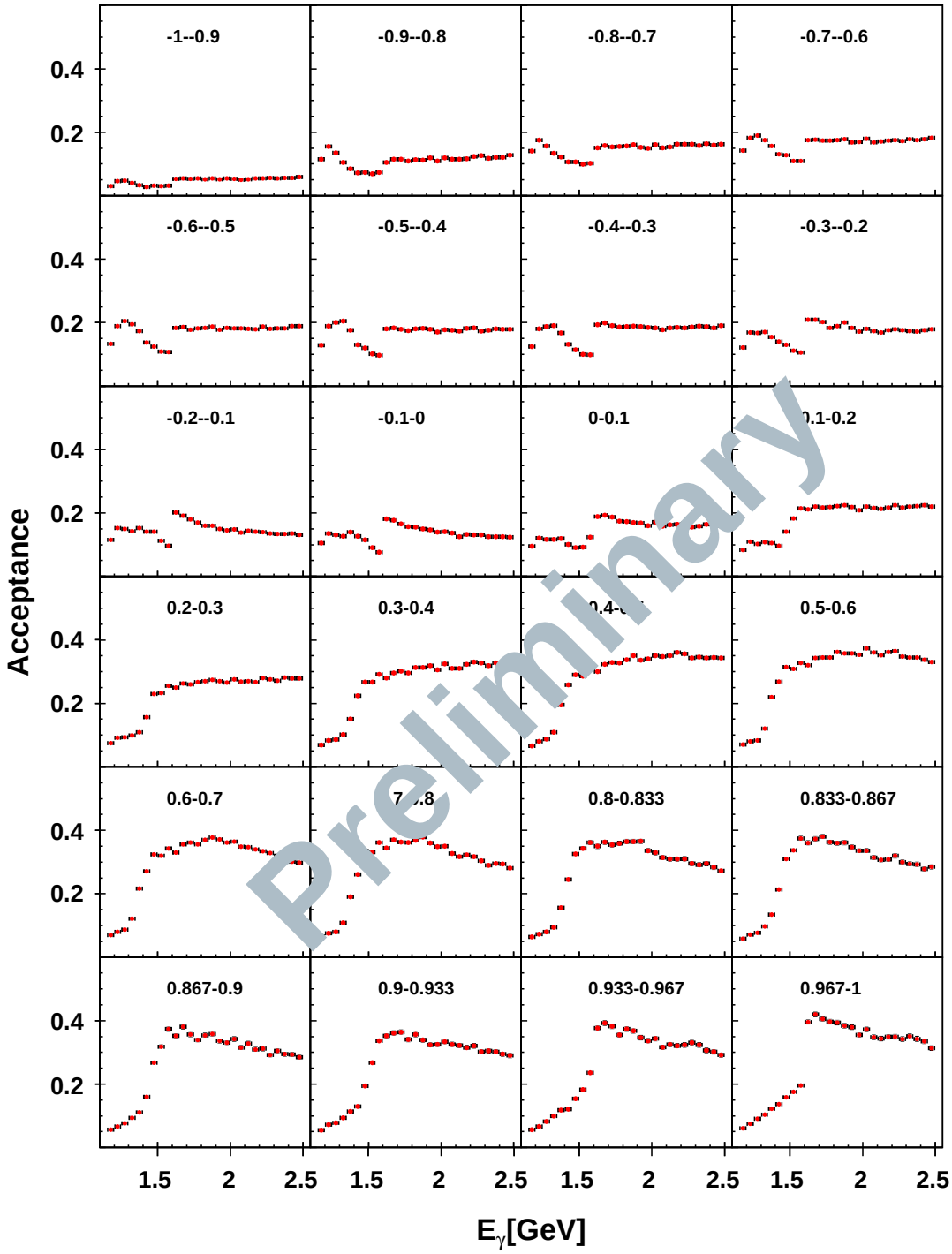


Figure 19: Total Monte Carlo Acceptance Plot. Each histogram in labeled with its range in $\cos\theta^{\omega}_{c.m.}$ and the horizontal axis is binned in incoming photon energy.

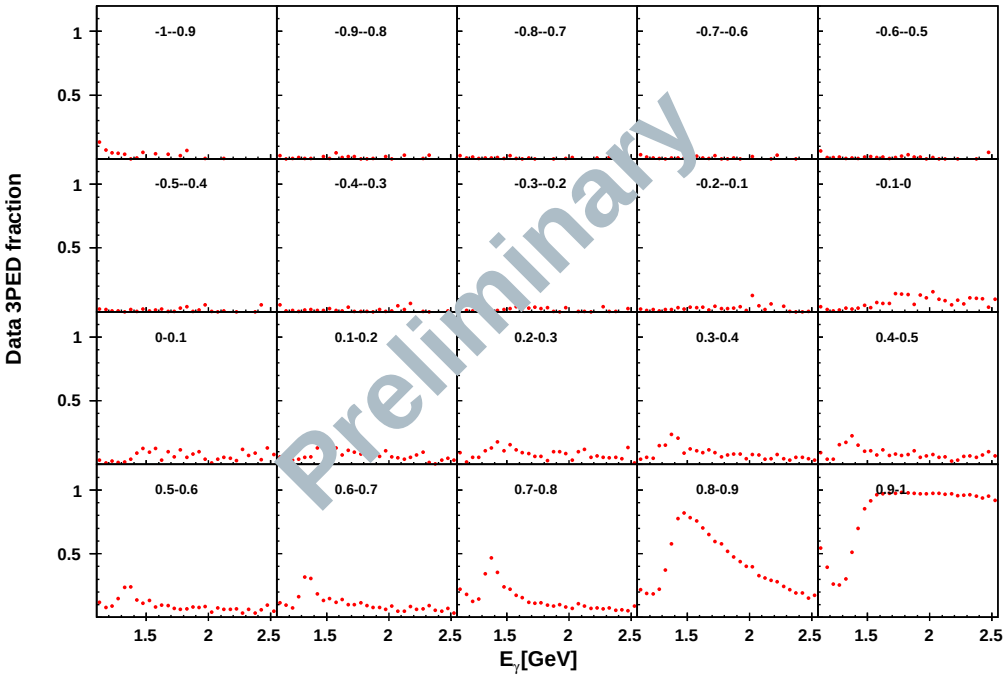


(a) Data Events

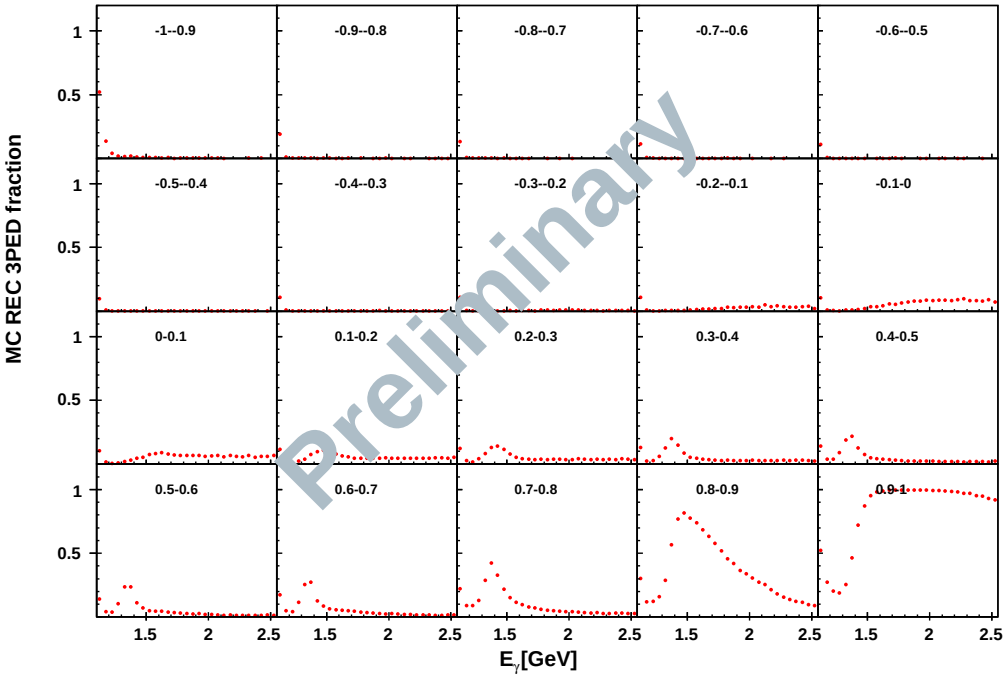


(b) Monte Carlo Reconstructed Events

Figure 20: Fraction of 3 PED Events Reconstructed. Corresponds to Figure 2. Each histogram in labeled with its range in $\cos\theta^{\omega}_{c.m.}$ and the horizontal axis is binned in incoming photon energy.

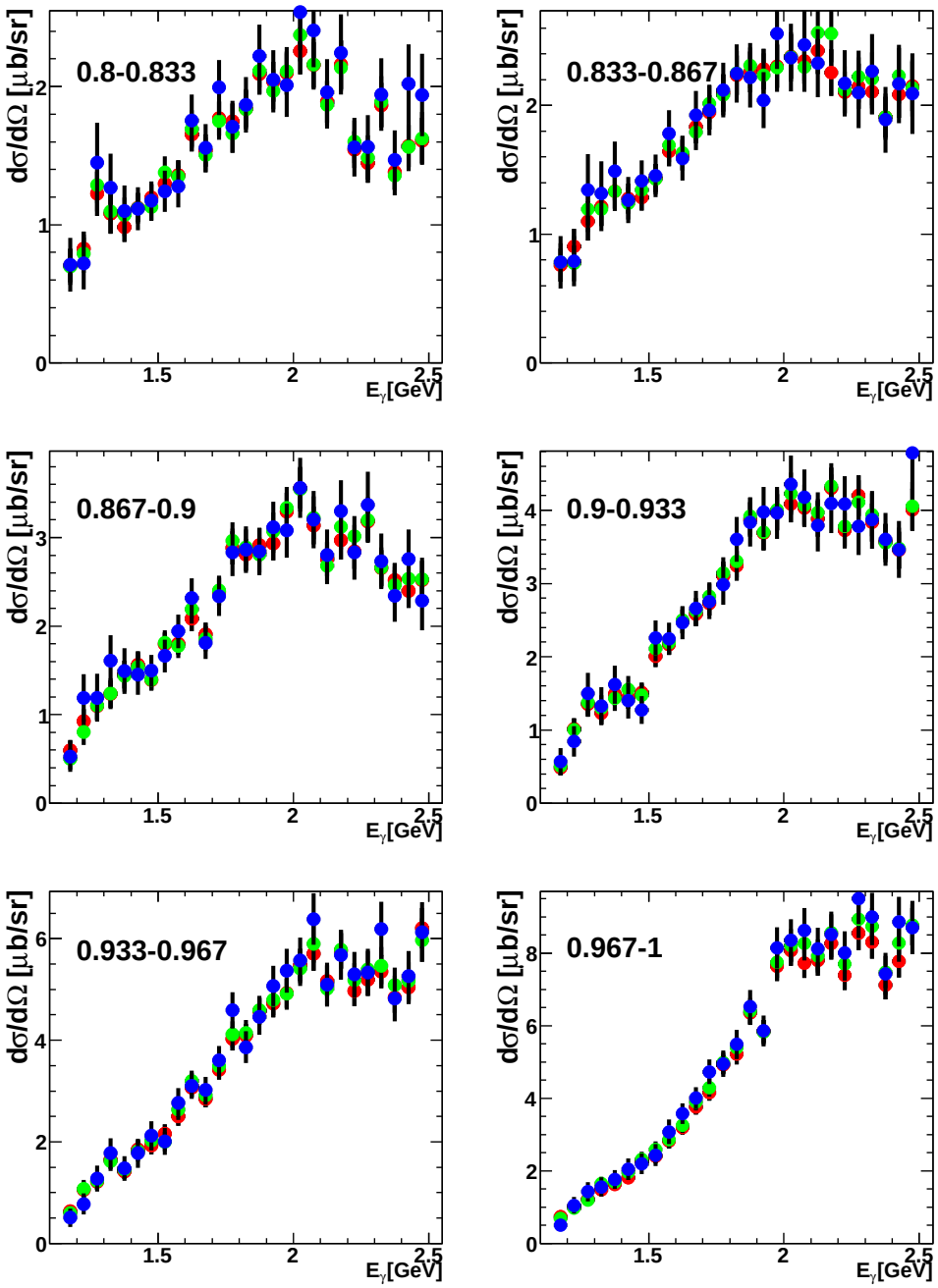


Figure 21: Confidence Level Cut comparisons for the $\cos\theta^{\omega}_{c.m.} > 0.8$ bins. ● corresponds to $CL_{p\pi^0\gamma} > 0.005$ (Final Cut Value), ● corresponds to $CL_{p\pi^0\gamma} > 0.01$, ● corresponds to $CL_{p\pi^0\gamma} > 0.1$, and ● corresponds to $CL_{p\pi^0\gamma} > 0.5$

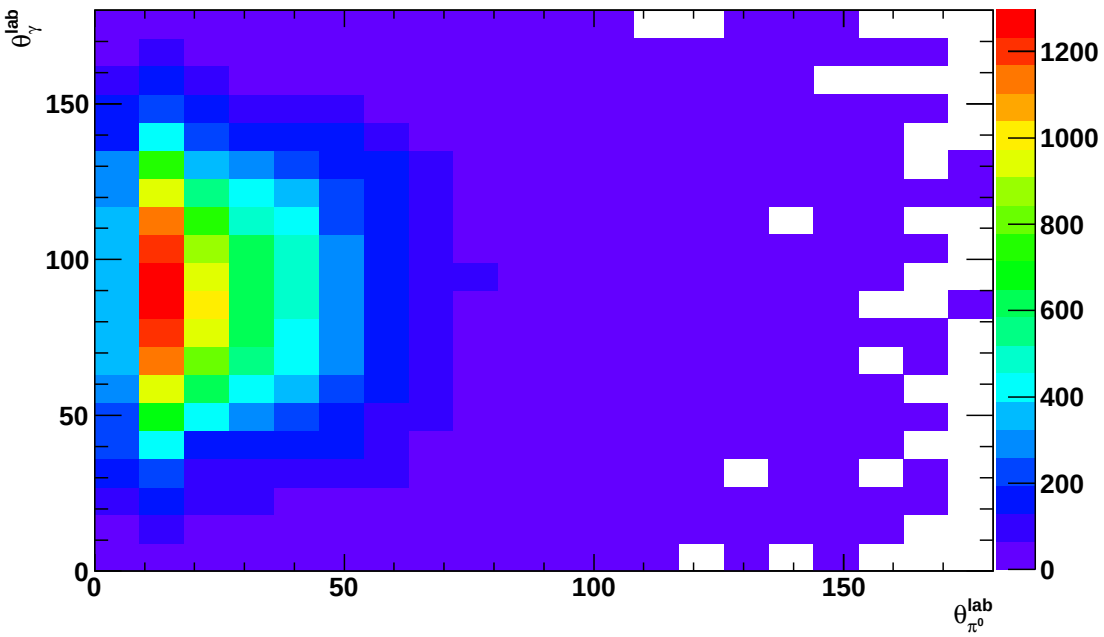


Figure 22: Forward Angle, High Energy Grid of Detected Angles of the $\omega$ Decay in the Lab Frame. The histogram is a sum over all incoming photon energies above 1600 MeV and only the $\cos\theta^{\omega}_{c.m.} = 0.9 - 1.0$ bin. Qvalue background subtracted.

# 5 Background Reactions

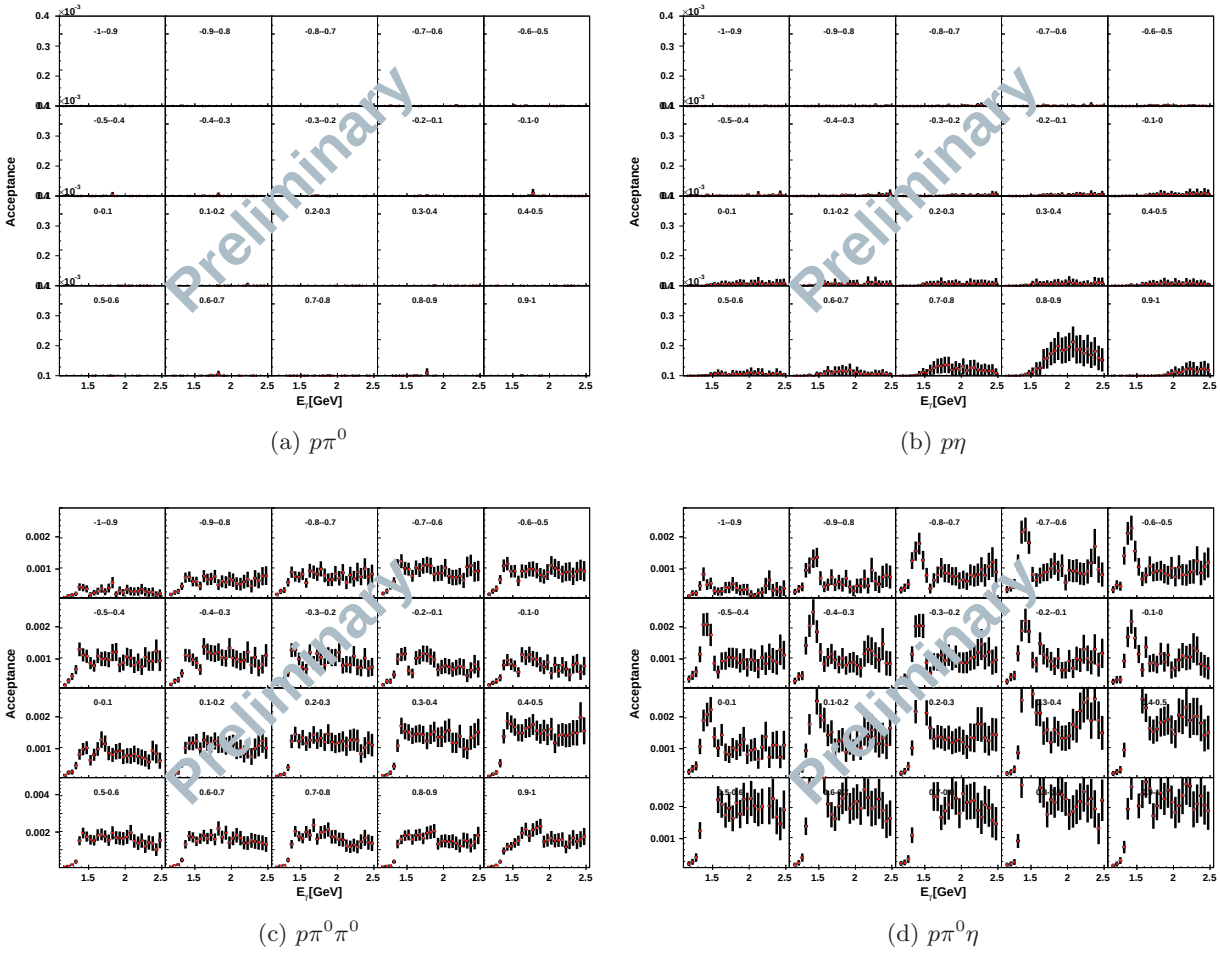


(a) $p\pi^0$ (b) $p\eta$

(c) $p\pi^0\pi^0$ (d) $p\pi^0\eta$

Figure 23: Monte Carlo Acceptance of Possible Background Reactions. Each histogram in labeled with its range in $\cos\theta^{\omega}_{c.m.}$ and the horizontal axis is binned in incoming photon energy. After all cuts.

To estimate the contributions from background reactions, the Monte Carlo acceptance for each reaction has been calculated by using phase space distributed Monte Carlo output and subjecting them to all the reconstruction and kinematic cuts that the original $p\omega$ events were subjected to. The acceptances for possible background reactions are shown in Figure 23. The reaction acceptance seems to be small in the single meson reactions, but become somewhat significant in $p\pi^0\pi^0$ and $p\pi^0\eta$ reactions. To give an estimate of the fraction of data events that could be due to these background events, the formula

$$f_i = \frac{1}{N_{data}} \frac{\sigma^i_{total}}{N_{bins}} R^i_B \mathcal{FT}$$

was used to make the histograms in Figure 24, where $\frac{\sigma^i_{total}}{N_{bins}}$ is the space averaged differential cross section for reaction $i$, $R^i_B$ is the branching ratio for reaction $i$ to an all photon final state (in the

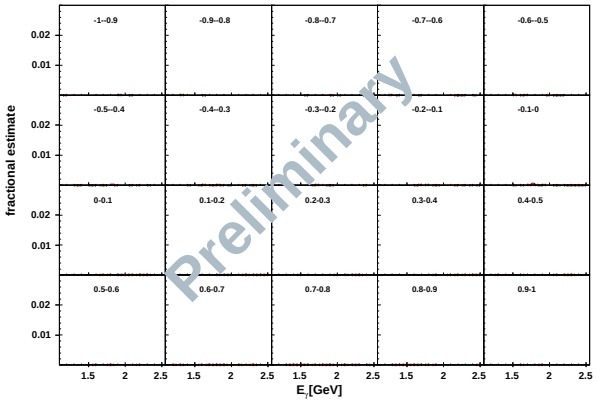


(a) $p\pi^0$

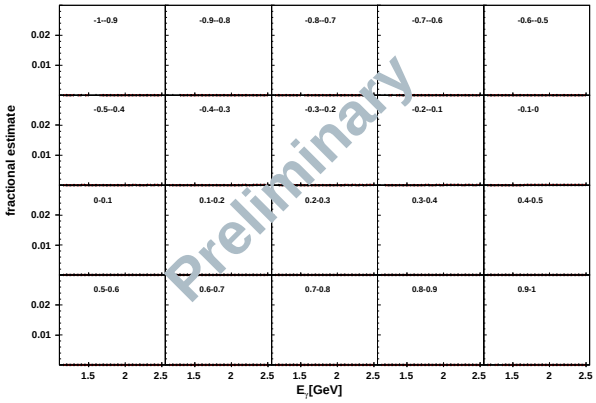


(b) $p\eta$

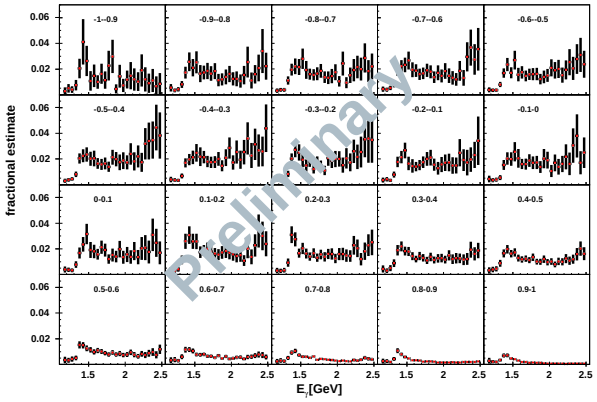


(c) $p\pi^0\pi^0$

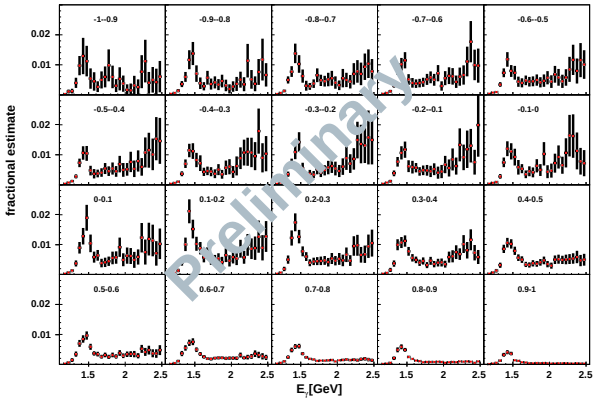


(d) $p\pi^0\eta$

Figure 24: Fractional estimate of the number of $p\omega$ events in this analysis that could be a background reaction. Each histogram in labeled with its range in $\cos\theta^{\omega}_{c.m.}$ and the horizontal axis is binned in incoming photon energy. After all cuts.

case of the $\eta$, to the two photon final state), $\mathcal{F}$ is the photon flux, $\mathcal{T}$ is the target density, and $N_{data}$ is the number of background subtracted $p\omega$ events found in this analysis in this kinematic bin. In this case, the space averaged differential cross section has been used because there is no suitable and reliable way to map the angles in each background reaction on to the angles of the $p\omega$ system.

The histograms in Figure 24 have been configured to show the significance of each reaction. According to these figures, background contributions from $p\pi^0$ and $p\eta$ are negligible. The contributions from $p\pi^0\pi^0$ and $p\pi^0\eta$ are on the single percent level and are essentially negligible.

# 6 Possible Systematic Error Sources

The possible sources of systematic error are:

- Target Shift

- Still present background events
- Qvalue errors
- 10% Flux Error
- 5.7% Monte Carlo Simulation Error
- Confidence Level Cut Error

# 7 Extra Data Plots

In this section, a few extra investigations are shown that did not make a difference in the final analysis but are important to the overall understanding of the data.

## 7.1 Crystal Barrel - TAPS Switch Range

The area where the Crystal Barrel detector and TAPS detector meet is called the Crystal Barrel - TAPS switch range. This area is defined as

$$Switch\ Range : 24\,\mathrm{deg} < \theta_{lab} < 36\,\mathrm{deg}$$

. To study this area's effect on the differential cross sections, Figure 25 is shown. This figure shows that the particles reconstructed in this area are properly modeled and this cut should no be used.

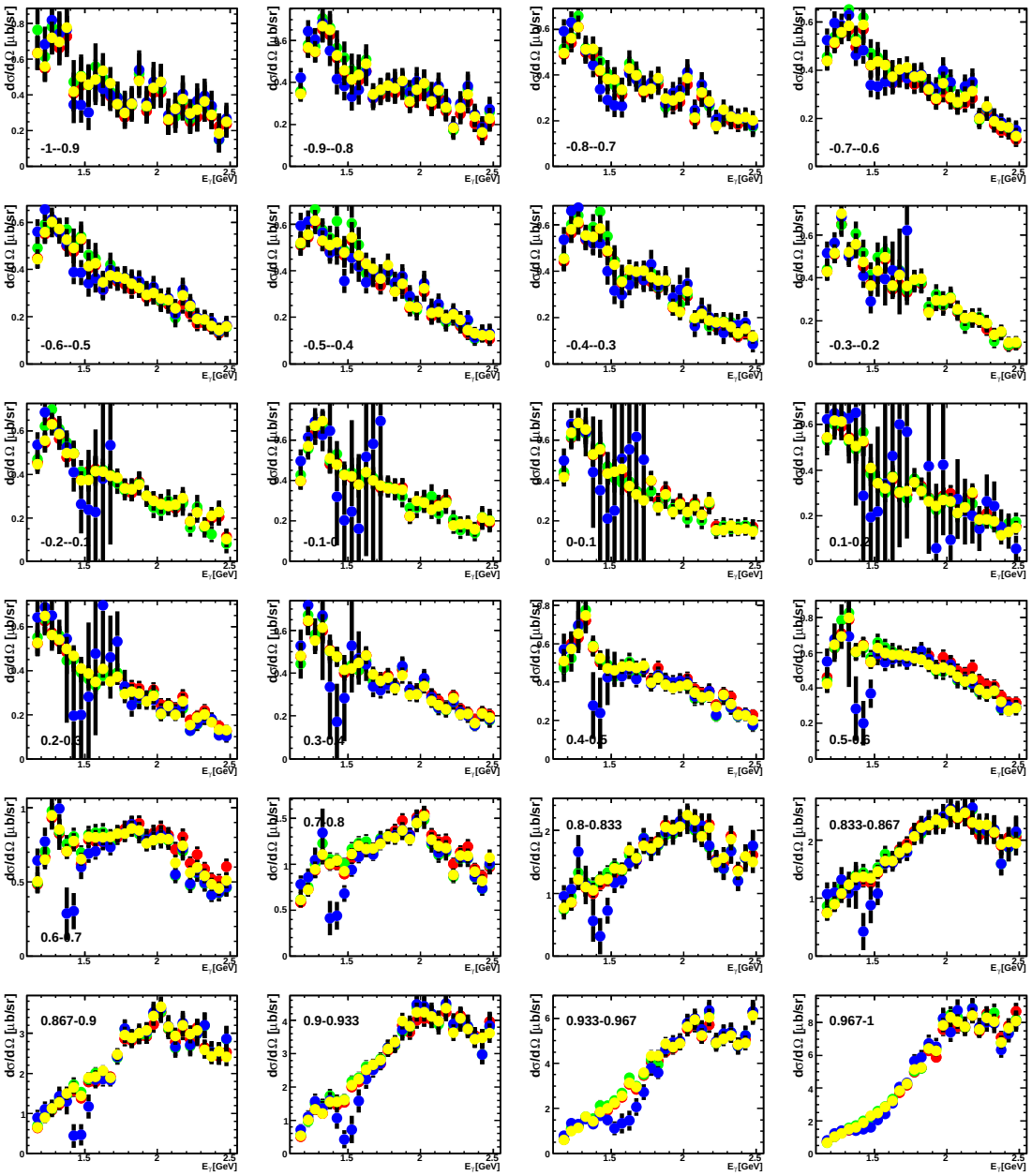


Figure 25: Crystal Barrel/TAPS Switch Range Cut Effects. Each histogram in labeled with its range in $\cos\theta^{\omega}_{c.m.}$ and the horizontal axis is binned in incoming photon energy. These histograms show the effect of cutting out different reconstructed particles in the region close to the Crystal Barrel/TAPS mating area on the angular differential cross sections from Figure 2. • is with no switch range cut. • is with all events with any reconstucted photons in the switch range are removed. • is with all events with any reconstucted photons or protons in the switch range are removed. • is with all events with any reconstucted pions in the switch range are removed.